

First observation of a planetary transit with the SPARC4 CCD: improved parameters for HATS-24b

JANDERSON M. OLIVEIRA,¹ EDER MARTIOLI,² AND MARCELO TUCCI-MAIA³

¹*Universidade Federal de Itajubá (UNIFEI), Av. BPS 1303, Itajubá, MG 37500-903, Brazil*

²*Laboratório Nacional de Astrofísica (LNA/MCTIC), Rua Estados Unidos 154, Itajubá, MG 37504-364, Brazil*

³*Universidad Diego Portales (UDP), Manuel Rodríguez Sur 415, Región Metropolitana, Santiago, Chile*

ABSTRACT

The photometric monitoring of planetary transits is an important method for the characterization of exoplanets. Transiting exoplanets allow measurements of the planetary radius and mass, providing information on the physical structure of the planet. Therefore, the parameters obtained with the transit method become fundamental for a comparative study of exoplanets in different planetary systems. In this work, we present the results obtained from observations of a transit event of the exoplanet HATS-24b using the new SPARC4 CCD mounted on the 1.6 m telescope of the Pico dos Dias Observatory (OPD). We have used Bayesian statistical inference to determine the physical parameters of this exoplanet, where we obtained a radius of $1.395 \pm 0.057 R_J$, mass of $2.26 \pm 0.17 M_J$, and density of $1.03 \pm 0.15 \text{ g cm}^{-3}$. We have combined our measurements of the central time of transit and orbital period with values from the literature to obtain an improved ephemeris for the transits of HATS-24b, $T_c = (2457948.709321 \pm 0.000039) + E(1.3484978 \pm 0.0000009)$. We have applied the differential analysis using a solar spectrum to recalculate the stellar surface parameters of HATS-24, where we obtained $T_{\text{eff}} = 6125 \pm 94 \text{ K}$, $\log g = 4.370 \pm 0.045 \text{ cm s}^{-2}$, and $[\text{Fe}/\text{H}] = -0.229 \pm 0.058 \text{ dex}$. This allowed us to estimate an equilibrium temperature for HATS-24b of $T_{\text{eq}} = 2166 \pm 53 \text{ K}$. The mass and radius of HATS-24b are consistent with the theoretical model of a pure helium-hydrogen planet at 1 Gy.

Keywords: stars: individual (HATS-24) — planetary systems — techniques: photometric

1. INTRODUCTION

Currently, there are about 3800 exoplanets detected according to the NASA Exoplanet Archive catalog ¹ (Akeson et al. 2013) of which about 3000 of these objects are transiting exoplanets. The majority of these transiting exoplanets have been detected by the Kepler mission (Borucki et al. 2003), which aimed at detecting terrestrial-type planets orbiting in the habitable zone of their host star. With the current ground-based instrumentation it is only possible to detect the transits of large planets in close-in orbits, which amounts a small fraction of all known transiting exoplanets. However, some of these systems still require follow-up observations to improve the characterization of the physical parameters of the exoplanets. The observations of several transit events can also improve the determination of the orbital period and allows one to search for transit time

variations, which may lead to the detection of additional planets in the system.

Therefore, the class of planets we are particularly interested are the hot Jupiters, which are planets likely formed in the outer regions of their protoplanetary discs and that migrated later to the inner regions, reaching orbits within approximately 0.1 AU of their host star (Fogg & Nelson 2006). The hot Jupiters have orbital periods of up to 10 days (Wang et al. 2015), which implies the transit duration of a few hours, allowing the observation of a full transit event during the night. The probability of occurrence of transits becomes smaller for longer period planets due to geometric characteristics of the system (Heller et al. 2009).

The hot Jupiter HATS-24b was recently discovered by Bento et al. (2017), through the Hungarian-made Automated Telescope Network-South survey (HATSouth) ² (Bakos et al. 2013). According to Bento et al. (2017), HATS-24b orbits a G or F type star, with magnitude

Corresponding author: Janderson M. Oliveira
jandersonfba.unifei@gmail.com, joliveira@lna.br

¹ <https://exoplanetarchive.ipac.caltech.edu/>

² <https://hatsouth.org/>

$V = 12.830$ and effective temperature of 5800 ± 300 K. Bento et al. (2017) measured a mass of HATS-24 b of $2.39^{+0.21}_{-0.12} M_J$ and a radius of $1.516^{+0.085}_{-0.065} R_J$, resulting in a density of $0.92 \pm 0.15 \text{ g cm}^{-3}$. The small amount of observations available in the literature and the low photometric precision of transits observed for this object have led us to select HATS-24b as a potential candidate for further follow-up. We were also motivated by the arrival of the new CCDs of the instrument Simultaneous Polarimeter and Rapid Camera in 4 bands (SPARC4) (Rodrigues et al. 2012). These CCDs have already been extensively tested in the lab by Bernardes et al. (2018) and needed to be tested on the telescope to verify the real photometric capabilities of this new instrument. SPARC4 is under construction and will be installed on the 1.6 m Perkin-Elmer telescope at the Pico dos Dias Observatory (OPD), Brazil. This is expected to be the workhorse instrument of OPD, and will be an excellent instrument to follow-up transits of hot Jupiters, where it is particularly interesting because it will operate in four photometric bands simultaneously, allowing one to constrain the transit depth at different wavelengths.

2. OBSERVATIONS

We have used the Exoplanet Transit Database - ETD³ (Poddaný et al. 2010) to predict the transit events of HATS-24b, which would be observable at OPD during the first semester of 2017. We have been granted time (project number OP2017A-026) to use the 1.6 m telescope to observe the transit of HATS-24 b on the night of July 13, 2017. We requested the new iXon Ultra 888 CCD of the SPARC4 project and the focal reducer. This set-up provides a field-of-view of $6.15' \times 6.15'$, which allows simultaneous observation of several comparison stars in the field (see Fig. 1). We performed continuous time series photometry in the I-filter from the start of the night until the target reached airmass above the observable limit. We started observations at about 2 hours and 46 minutes before the predicted start of the transit and ended at about 1 hour and 36 minutes after the predicted end of the transit. Initially, we used 20 seconds of exposure time, but we changed to 30 seconds after 30 minutes of observations to improve signal-to-noise. The observations were performed under near photometric conditions.

3. DATA REDUCTION

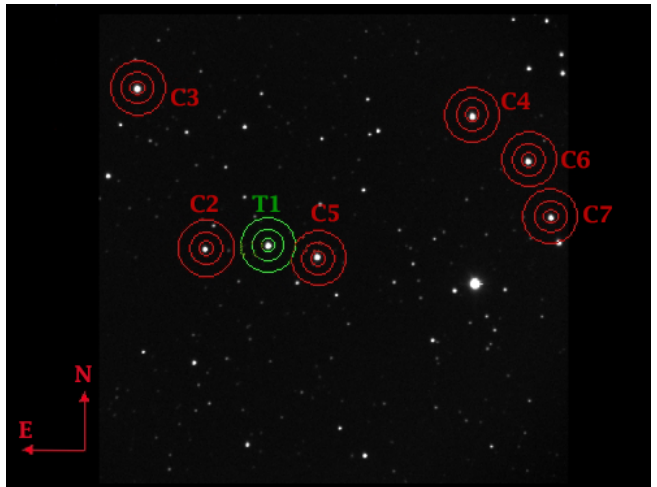


Figure 1. Sample image of the field-of-view observed ($6.15' \times 6.15'$). HATS-24 is labeled as T1 (in green), and the 6 comparison stars are labeled as C_n where $n = 2, \dots, 7$ (in red). For each star we present the circular apertures used for the star flux extraction and the concentric apertures used for the sky flux extraction.

We have used the software AstroImageJ⁴ (AIJ) (Collins et al. 2017) to reduce our data. We have obtained 30 bias exposures and 20 flat-field exposures. The AIJ software performs the bias subtraction and division by flat-field on each one of the 806 science exposures, where the bias and flat-field exposures were combined by the median. The AIJ performs flux extraction and calculates the differential photometry for multiple apertures, providing differential light curves for each comparison star with respect to the target. Although AIJ allows the analysis of the transit light curve, we performed the analysis using a software tool developed by us. Our tool can fit a model that accounts for the transit model and for trends in the light curves of each individual comparison star. In addition, our analysis implements Bayesian statistical inference to estimate the model parameters.

Fig. 1 presents a sample image of the field-of-view observed, where the green circles show the apertures used to extract the flux of our target (HATS-24, labeled as T1) and red circles show the apertures used for the comparison stars. We use an aperture radius of 11 pixels to extract the flux and an aperture between 25 pixels (inner radius) and 50 pixels (outer radius) to extract the sky flux. We have selected the six comparison stars based on the similarity of their magnitudes to the target (± 1.0 mag) as presented in Table 1. We have also used the Multi-Aperture (MA) mode of the AIJ, which recal-

³ <http://var2.astro.cz/ETD/>

⁴ <http://www.astro.louisville.edu/software/astroimagej/>

culates the centroid of the target and comparison stars for each individual image of the time series to allow for centering corrections.

4. ANALYSIS

We performed our analysis using an adapted version of the software developed by Martioli et al. (2018), which was initially developed for the study of secondary eclipses. We made the necessary modifications in the code to apply the same methodology for the study of primary transits. This software, written in Python, uses the BATMAN package developed by Kreidberg (2015), which implements the geometric model of Mandel & Agol (2002) for the calculation of the light curve for the transit model. It uses Bayesian inference to estimate the posterior probability of the transit model parameters and also the trend model coefficients for each comparison star. It uses the package EMCEE (Foreman-Mackey et al. 2013) to generate samples based on a priori information of the physical parameters together with the data obtained. The EMCEE package uses the Markov Chain Monte Carlo sampler (MCMC) applying the method proposed by Goodman & Weare (2010). We use the parameters obtained by Bento et al. (2017) as a priori information as presented in Table 2. A normal probability distribution was adopted for the following parameters: central time of transit (T_c), orbital period (P), planet-to-star radius (R_p/R_*), semi-major axis (a_p/R_*), orbital inclination (i), and limb darkening coefficients (u_1 and u_2), where we assume a quadratic limb darkening (Kreidberg 2015). The following parameters are fixed as constant values: eccentricity ($e = 0$) and longitude of periastron ($\omega = 90^\circ$).

5. RESULTS

5.1. Transit Parameters

For each comparison star we have used an independent quadratic polynomial model to account for systematic trends in the light curves. Fig. 2 presents the data obtained from the differential photometry of HATS-24 with respect to each comparison star used in our analysis. Fig. 2 also presents the fit models (green line), which include the trend models and the global transit model. Notice that each light curve has the transit signature and, in addition, a trend that is well modeled by a quadratic polynomial of the form $P_j(t) = a_j t^2 + b_j t + c_j$, for j being the index for each comparison star. All the coefficients a_j , b_j , and c_j are obtained by Bayesian inference analysis simultaneous to the transit parameters.

To determine the posterior probability distribution of each parameter, 5000 iterations were performed through the MCMC sampler, where the initial 4000 iterations

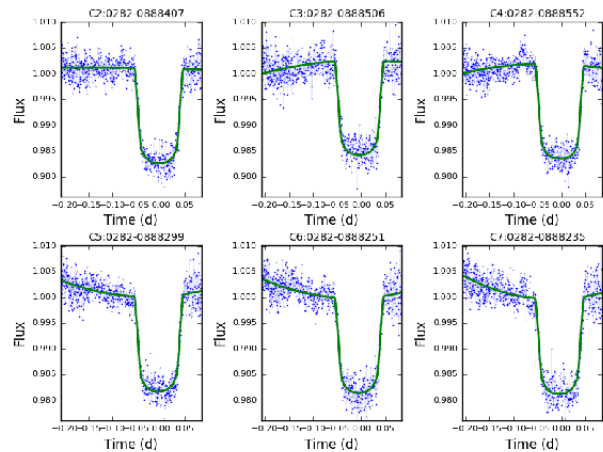


Figure 2. Each panel shows the differential light curve (blue dots) for each comparison star and the fit model (green line), where the model includes the trend and the global transit model.

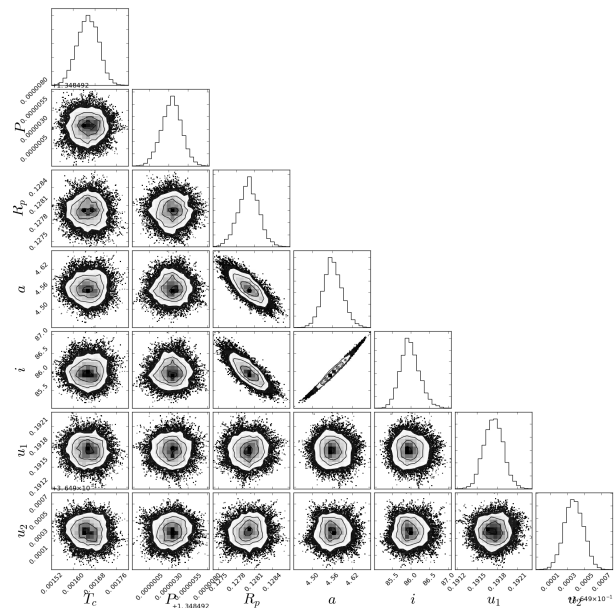


Figure 3. MCMC diagnostics: pairwise plots of the parameters in the posterior distribution obtained from the last 1000 iterations of the MCMC sampler; the panels in the main diagonal show the one-dimensional projection of the posterior probability distribution for each parameter of the transit model.

have been discarded as burn-in. Fig. 3 presents the MCMC diagnostic plots, i.e., the pairwise plots of the parameters in the posterior distribution and the one-dimensional projection of the posterior probability distribution for each transit model parameter. This analysis was also obtained for the parameters of the trend polynomials of each comparison star, but for simplicity we only show here the parameters of the transit.

Table 1. Target and comparison stars used in the differential photometry.

Index	ID (NOMAD-1)	RA (hh:mm:ss.sss)	DEC (\pm dd:mm:ss.ss)	I-MAG (USNO-B1.0)
T1	0282-0888453	17:55:33.779	-61:44:50.38	12.03
C2	0282-0888407	17:55:28.688	-61:44:59.60	11.90
C3	0282-0888506	17:55:40.194	-61:44:52.02	12.86
C4	0282-0888552	17:55:46.887	-61:42:54.24	11.66
C5	0282-0888299	17:55:12.608	-61:43:18.20	11.70
C6	0282-0888251	17:55:06.769	-61:43:51.54	12.26
C7	0282-0888235	17:55:04.544	-61:44:32.88	12.35

Table 2. Priors obtained from Bento et al. (2017).

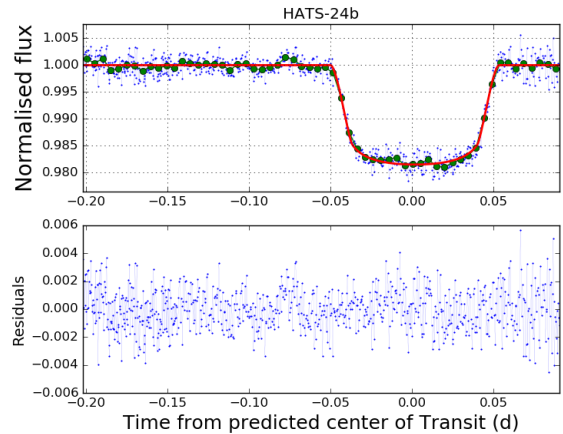
Parameter	Prior Type	Initial guess	Unit
T_c	Normal	2457948.708 ± 0.010	BJD
P	Normal	$1.3484954 \pm 1.3e-06$	days
R_p/R_\star	Normal	0.1307 ± 0.003	-
a_p/R_\star	Normal	4.67 ± 0.1	-
i	Normal	86.6 ± 1.2	degrees
e	Fixed	0.	degrees
ω	Fixed	90.	degrees
u_1	Normal	0.1919 ± 0.0100	-
u_2	Normal	0.3654 ± 0.0100	-

Table 3. Final fit parameters of HATS-24b.

Parameter	Value	Unit
T_c	$2457948.709321^{+0.000041}_{-0.000038}$	BJD
P	$1.34849540^{+0.0000013}_{-0.0000012}$	days
R_p/R_\star	0.12801 ± 0.00017	-
a_p/R_\star	$4.561^{+0.027}_{-0.030}$	-
i	$85.97^{+0.23}_{-0.28}$	degrees
e	0	-
ω	90	degrees
u_1	0.19187 ± 0.00017	-
u_2	0.36543 ± 0.00009	-

The final value of each parameter is calculated as the 50th percentile of the posterior distribution generated by the MCMC, and the uncertainties are calculated as the mean value between the 50th percentiles minus 16 and the 84th percentiles minus 50. Table 3 presents the final results for the transit parameters.

Fig. 4 shows the final results of our analysis, where we present the mean of all trend-subtracted light curves of HATS-24 (blue dots), the transit model (red line) using the fit parameters from Table 3, and the binned data

**Figure 4.** Top panel shows the reduced light curve of HATS-24 (blue dots), the binned data (green circles), and the fit transit model (red line). Bottom panel shows the residuals.

(15 points per bin) with uncertainties calculated by the standard deviation. Fig. 5 shows the probability distribution of residuals, where we fit a normal distribution $N(\mu, \sigma)$. We obtained $\mu = 2 \times 10^{-6}$ and $\sigma = 0.00149$. Notice that the distribution of residuals is well described by a normal distribution, with zero mean and a standard deviation of $\sigma = 0.15\%$.

5.2. Ephemeris

Using the results presented in Section 5 for the central time of transit (T_c), and combining the information available in the literature for two other transit events of HATS-24b, we have obtained an improved ephemeris for the transits of this exoplanet. We have found two reported transits of HATS-24b in the literature; one from Bento et al. (2017), and another by Phil Evans published in the catalog Exoplanet Transit Database (Poddaný et al. 2010). Table 4 shows the details of these three observed transits of HATS-24b.

We have used GaussFit (Jefferys et al. 1988) to perform a linear fit to the data presented in Table 4. The model is given by $T_c = T_0 + E \times P$, for E being the epoch from the time of the transit reported in this work, T_0 be-

Table 4. Observed transits of HATS-24 b

T_c (BJD - 2457000)	Epoch	O - C (days)	Duration of Transit ^a (minutes)	Reference
038.47327 ± 0.00038	-675	-0.000048 ± 0.00038	145.2 ± 2.2	Bento et al. (2017)
608.89160 ± 0.00096	-252	0.0037 ± 0.00096	142.2 ± 3.3	Phil Evans ^b
948.7093208 ± 0.000039	0	-0.0000079 ± 0.000039	146.3 ± 1.4	This Work

^a The duration of transit is calculated using the relation presented in Winn (2010)

^b <http://var2.astro.cz/tresca/transit-detail.php?id=1470685388>

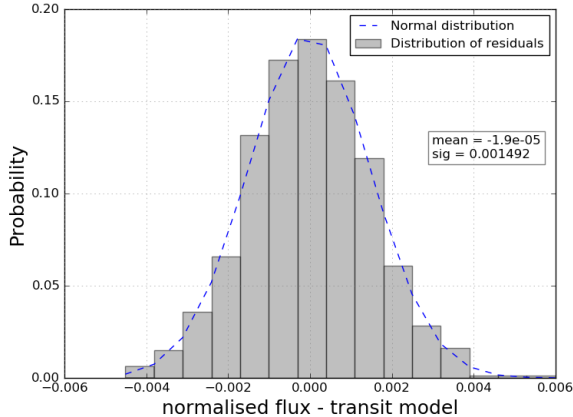


Figure 5. Probability distribution of residuals (gray bars), and the fit normal distribution (blue dashed line), $N(\mu, \sigma)$, where $\mu = 2 \times 10^{-6}$ and $\sigma = 0.001490$.

ing the central time of transit at initial epoch $E = 0$, and P being the orbital period. GaussFit performs a least squares robust analysis which takes into account the errors in the observations. We obtained the following ephemeris for the central time of transit:

$$T_c = (2457948.709321 \pm 0.000039) + E(1.3484978 \pm 0.0000009), \quad (1)$$

where we have adopted the value of T_0 as our measured value of T_c because it is more precise than the fit value of T_0 . The orbital period obtained in this analysis represents the most precise value at the moment. Fig. 6 presents the observed minus computed (O-C) values for the central time of transit (T_c) as a function of epoch. Notice that the value of T_c measured by Phil Evans is more than 3σ away from the predicted value. We believe that this is likely due to a systematic error not accounted for in his measurements, otherwise it should represent some variation in the central time of transit. To confirm the latter hypothesis it requires further follow-up of the transits of HATS-24b. A possible variation in the central time of transit may indicate the presence of additional planets in the system.

5.3. Stellar Parameters

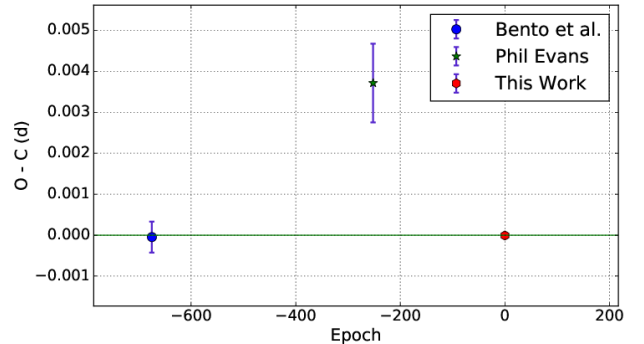


Figure 6. Observed minus computed (O-C) diagram of the central times of transits as a function of epoch for the three transit events of HATS-24b.

We have used the high resolution spectrum of HATS-24, which was kindly provided by the authors of Bento et al. (2017), in addition to the Vesta spectrum obtained from the ESO archive (program id 090.D-0133(A)) to recalculate the stellar parameters of HATS-24. Both spectra were observed with the FEROS spectrograph (Kaufer et al. 1999), where the spectrum of HATS-24 has a maximum signal-to-noise ratio (SNR) of ~ 40 , and the Vesta spectrum has $\text{SNR} \sim 115$.

The stellar parameters were initially obtained through the standard spectroscopic methods, i.e., through the excitation and ionization equilibrium using the equivalent widths (EW) of Fe I and Fe II lines (Meléndez et al. 2009; Ramírez et al. 2014; Tucci Maia et al. 2014, 2016). This is done to ensure that the atmospheric model returns the same iron abundances for every line, independently of its excitation potential, ionization state or line strength. Since HATS-24 is a solar type star, we can use the solar spectrum, obtained from the reflected light of Vesta, as reference for the differential analysis. The EWs were measured manually with the task `splot` in IRAF, by fitting Gaussian profiles, and the abundances were determined using the 2014 version of the LTE code MOOG (Snedden 1973) adopting the MARCS grid of 1D-LTE model atmospheres (Gustafsson et al. 2008). Since the spectra available have poor SNR for this kind of analysis, we decided to use the trigonometric gravity, $\log g = 4.37 \pm 0.045$ cm s⁻², obtained with the apparent

Table 5. Stellar surface parameters obtained for HATS-24 determined with EW differential analysis.

Parameter	Symbol	HATS-24	Unit
effective temperature	T_{eff}	6125 ± 94	K
surface gravity	$\log g$	4.370 ± 0.045	cm s^{-2}
metallicity	$[\text{Fe}/\text{H}]$	-0.229 ± 0.058	dex
microturbulence velocity	ν	1.75 ± 0.15	km s^{-1}

Table 6. HATS-24 parameters estimated with the isochrones method.

Parameter	Symbol	Mode	Mean	Unit
Age	-	$3.7^{+2.0}_{-1.8}$	3.9 ± 1.8	Gy
Luminosity	$\log L_{\star}$	0.190 ± 0.021	0.190 ± 0.021	L_{\odot}
Abs. mag	M_V	4.330 ± 0.051	4.332 ± 0.053	mag
Mass	M_{\star}	$1.070^{+0.032}_{-0.046}$	1.058 ± 0.037	M_{\odot}
Radius	R_{\star}	$1.120^{+0.044}_{-0.047}$	1.115 ± 0.043	R_{\odot}

magnitude from Simbad (Wenger et al. 2000) and the parallax from GAIA (Gaia Collaboration et al. 2018). By fixing the gravity value, we parse through stellar models to find the best fit values of effective temperature (T_{eff}), metallicity ($[\text{Fe}/\text{H}]$), and microturbulence velocity (ν).

We employed the Python code `q2`⁵ (Ramírez et al. 2014) to determine the chemical abundances, by calling MOOG routines, to perform the necessary differential analysis. The uncertainties in the stellar parameters were determined taking into account the observational (due to uncertainties in the EW measurement) and systematic (from the degeneracy of the stellar parameters) uncertainties.

Fig. 7 shows the excitation and ionization equilibrium of Fe I and Fe II lines. The final solution for the stellar surface parameters of HATS-24 determined by the EW differential analysis are presented in Table 5.

The age, luminosity, absolute magnitude, mass, and radius, presented on Table 6, have been calculated using the modified Yonsei-Yale (YY) isochrones (Yi et al. 2001), as described in Ramírez et al. (2013, 2014). These parameters are estimated from the probability distribution functions shown in Fig. 8. For further calculations using the stellar parameters we have adopted the mode of the distribution of each parameter (green dashed lines in Fig. 8). Fig. 9 presents the most likely isochrone (age of 3.7 Gy and metallicity of $[\text{Fe}/\text{H}] = -0.24$ dex) that fits the parameters of HATS-24 obtained from our analysis.

⁵ <https://github.com/astroChasqui/q2>

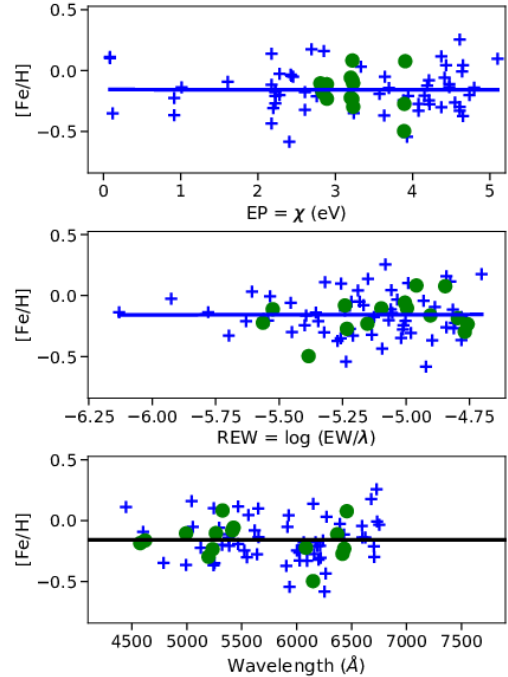


Figure 7. Excitation and ionization equilibrium of Fe abundances for HATS-24 using the solar spectrum as reference star. Crosses represent Fe I and filled circles Fe II.

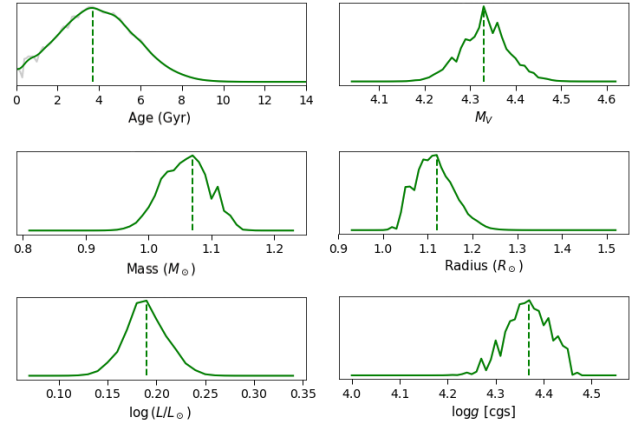


Figure 8. Green solid lines show the probability distribution for HATS-24 parameters based on Yonsei-Yale isochrones. Green dashed lines show the mode of each distribution.

5.4. Derived Parameters of HATS-24b

Combining the transit parameters presented in Section 5.1 with the stellar parameters presented in Section 5.3 we were able to calculate the planetary parameters presented in Table 7. The equilibrium temperature was calculated as in Heng & Demory (2013), where we assumed an albedo of $A = 0.1$, and an uniform heat redistribution, i.e., $f = 1/2$.

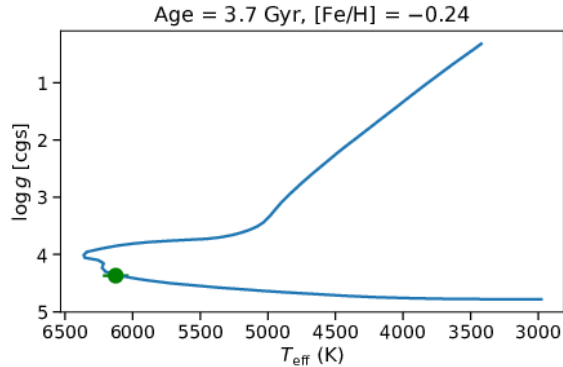


Figure 9. Blue line shows the YY isochrone in the T_{eff} vs. $\log g$ space for an age of 3.7 Gy and metallicity of $[\text{Fe}/\text{H}] = -0.24$ dex. Green point shows the location of HATS-24, where we have used the fit parameters from Table 5.

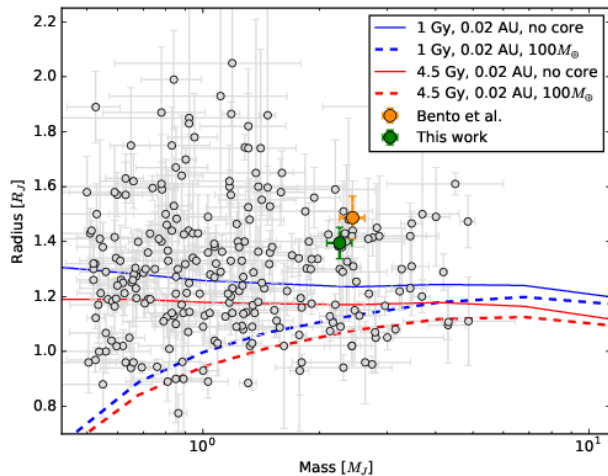


Figure 10. Mass-radius relation for hot Jupiters, where we include exoplanets with masses in the range $0.5 M_J < M_p < 5 M_J$ and with periods shorter than 10 days (source: NASA Exoplanet Archive catalog). The orange point represents the previous result from Bento et al. (2017) for HATS-24b and the green point represents our result. We present theoretical models for planet structures from Fortney et al. (2007) where in blue are the 1Gy models and in red are the 4.5Gy models. Both models are presented for both no core (solid lines) and $100 M_{\oplus}$ core (dashed lines) scenarios.

Figure 10 presents the mass-radius relation for hot Jupiters, where we included exoplanets with masses in the range $0.5 M_J < M_p < 5 M_J$ and with periods shorter than 10 days. We present theoretical models for planet structures obtained from Fortney et al. (2007). Notice that our measurements confirm that HATS-24b is an inflated hot Jupiter, however the new estimation for the radius is now less than 3σ above the model for a pure helium-hydrogen planet at approximately 1 Gy.

Table 7. Derived parameters for HATS-24b

Parameter	Value	Unit
M_p	2.26 ± 0.17	M_J
R_p	1.395 ± 0.057	R_J
ρ_p	1.03 ± 0.15	g cm^{-3}
a_p	0.0238 ± 0.0010	AU
T_{eq}	2166 ± 53	K

6. CONCLUSIONS

We have presented observations of a transit event of the exoplanet HATS-24b, where we have used for the first time one of the new CCD cameras of the SPARC4 instrument. We present differential photometry time-series covering an entire transit event of HATS-24b. We obtained a final photometric precision of 0.15% for a $V=12.83$ mag star. This confirms that SPARC4 will be an excellent instrument for relative high-precision photometry with the potential for the detection and characterization of transits of hot Jupiters. Notice that we obtained the transit depth of HATS-24b with precision of 170 ppm. The four simultaneous channels of SPARC4 will permit observations of transits simultaneously in four photometric bands, allowing one to constrain models of transmission spectroscopy of transiting planets.

We have presented a robust approach using Bayesian statistical inference to determine the planetary parameters with better precision compared to previous results from Bento et al. (2017). The improved precision for the central time of transit combined with data from the literature allowed us to calculate a new ephemeris for the transits of HATS-24b, improving the orbital period and the prediction of future transit events for this object. Finally, we have used available high resolution spectra from HATS-24 and Vesta observed with the FEROS spectrograph to perform a differential analysis to obtain the stellar parameters of HATS-24. We have found an effective temperature of 6125 ± 94 K, confirming that this star is likely a G0 type with an age of 3.9 ± 1.8 Gyr, relatively older than previous measurements. Combining the stellar analysis with our fit transit parameters we obtained a new estimate for the following parameters of the planet: mass, radius, semi-major axis, equilibrium temperature, and density. Our results are more consistent with the theoretical models for planet structures, although the radius of HATS-24b still appears to be inflated compared to any of the models presented.

ACKNOWLEDGEMENTS

We would like to thank the LNA/OPD staff for their support during the observations, and for promptly responding to our requests. J. M. Oliveira acknowledges

the financial support from CNPq agency under the PCI project, process number 454781/2015-6. We would also

like to thank J. Bento for providing the spectroscopic data of HATS-24.

REFERENCES

- Akeson, R. L., Chen, X., Ciardi, D., et al. 2013, *PASP*, 125, 989
- Bakos, G. Á., Csubry, Z., Penev, K., et al. 2013, *PASP*, 125, 154
- Bento, J., Schmidt, B., Hartman, J. D., et al. 2017, *MNRAS*, 468, 835
- Bernardes, D. V. and Martioli, E. and Rodrigues, C. V., 2018, *PASP*, 130, 991, pp. 095002
- Borucki, W. J., Koch, D., Basri, G., et al. 2003, *Earths: DARWIN/TPF and the Search for Extrasolar Terrestrial Planets*, ed. M. Fridlund, T. Henning, & H. Lacoste (ESA SP- 539; Noordwijk: ESA), 69
- Collins, K. A., Kielkopf, J. F., Stassun, K. G., & Hessman, F. V. 2017, *AJ*, 153, 77
- Fogg, M. J., & Nelson, R. P. 2006, *International Journal of Astrobiology*, 5, 199
- Foreman-Mackey, D., Hogg, D. W., Lang, D., & Goodman, J. 2013, *PASP*, 125, 306
- Fortney, J. J., Marley, M. S., & Barnes, J. W. 2007, *ApJ*, 659, 1661
- Gaia Collaboration, Brown, A. G. A., Vallenari, A., et al. 2018, *A&A*, 616, A1
- Goodman, J., & Weare, J. 2010, *Communications in Applied Mathematics and Computational Science*, Vol. 5, No. 1, p. 65-80, 2010, 5, 65
- Gustafsson, B., Edvardsson, B., Eriksson, K., et al. 2008, *A&A*, 486, 951
- Heller, R., Mislis, D., & Antoniadis, J. 2009, *A&A*, 508, 1509
- Heng, K., e Demory, B.-O. 2013, *ApJ*, 777, 100
- Jefferys, W. H., Fitzpatrick, M. J., & McArthur, B. E. 1988, *Celestial Mechanics*, 41, 39
- Kaufer, A., Stahl, O., Tubbesing, S., et al. 1999, *The Messenger*, 95, 8
- Kreidberg, L. 2015, *PASP*, 127, 1161
- Martioli, E., Colón, K. D., Angerhausen, D., et al. 2018, *MNRAS*, 474, 4264
- Mandel, K., & Agol, E. 2002, *ApJL*, 580, L171
- Mayor, M., & Queloz, D. 1995, *Nature*, 378, 355
- Meléndez, J., Asplund, M., Gustafsson, B., & Yong, D. 2009, *ApJL*, 704, L66
- Poddaný, S., Brát, L., & Pejcha, O. 2010, *NewA*, 15, 297
- Ramírez, I., Meléndez, J., Bean, J., et al. 2014, *A&A*, 572, A48
- Ramírez, I., Allende Prieto, C., & Lambert, D. L. 2013, *ApJ*, 764, 78
- Rodrigues, C. V., Taylor, K., Jablonski, F. J., et al. 2012, *Proc. SPIE*, 8446, 844626
- Snedden, C. A. 1973, Ph.D. Thesis,
- Tucci Maia, M., Meléndez, J., & Ramírez, I. 2014, *ApJL*, 790, L2
- Tucci Maia, M., Ramírez, I., Meléndez, J., et al. 2016, *A&A*, 590, A32
- Wang, J., Fischer, D. A., Horch, E. P., & Huang, X. 2015, *ApJ*, 799, 229
- Wenger, M., Ochsenbein, F., Egret, D., et al. 2000, *A&AS*, 143, 9
- Winn, J. N. 2010, arXiv:1001.2010
- Yi, S., Demarque, P., Kim, Y.-C., et al. 2001, *ApJS*, 136, 417
- Zacharias, N., Monet, D. G., Levine, S. E., et al. 2004, *Bulletin of the American Astronomical Society*, 36, 48.1